2013

Rate- and Temperature-Dependent Fracture Characteristics of Asphaltic Paving Mixtures

Soohyok Im
University of Nebraska - Lincoln, sooim@huskers.unl.edu

Yong-Rak Kim
Kyung Hee University, yong-rak.kim@unl.edu

Hoki Ban
University of Nebraska - Lincoln, hban2@unlnotes.unl.edu

Journal of Testing and Evaluation, Vol. 41, No. 2, 2013
Available online at www.astm.org
doi:10.1520/JTE20120174

Soohyok Im,[1] *Yong-Rak Kim,*[2] *and Hoki Ban*[3]

Rate- and Temperature-Dependent Fracture Characteristics of Asphaltic Paving Mixtures

REFERENCE: Im, Soohyok, Kim, Yong-Rak, and Ban, Hoki, "Rate- and Temperature-Dependent Fracture Characteristics of Asphaltic Paving Mixtures," *Journal of Testing and Evaluation*, Vol. 41, No. 2, 2013, pp. 1–12, doi:10.1520/JTE20120174. ISSN 0090-3973.

ABSTRACT: Cracking in asphaltic pavement layers causes primary failure of the roadway structure, and the fracture resistance and characteristics of asphalt mixtures significantly influence the service life of asphaltic roadways. A better understanding of the fracture process is considered a necessary step to the proper development of design-analysis procedures for asphaltic mixtures and pavement structures. However, such effort involves many challenges because of the complex nature of asphaltic materials. In this study, experiments were conducted using uniaxial compressive specimens to characterize the linear viscoelastic properties and semi-circular bending (SCB) specimens to characterize fracture behavior of a typical dense-graded asphalt paving mixture subjected to various loading rates and at different temperatures. The SCB fracture test was also incorporated with a digital image correlation (DIC) system and finite-element model simulations including material viscoelasticity and cohesive-zone fracture to effectively capture local fracture processes and resulting fracture properties. The test results and model simulations clearly demonstrate that: (1) the rate- and temperature-dependent fracture characteristics need to be identified at the local fracture process zone, and (2) the rate- and temperature-dependent fracture properties are necessary in the structural design of asphaltic pavements with which a wide range of strain rates and service temperatures is usually associated.

KEYWORDS: asphalt mixtures, fracture, viscoelasticity, cohesive zone, pavement performance

Introduction

Various asphalt-pavement distresses are related to fracture, including fatigue cracking (both top-down and bottom-up), thermal (transverse) cracking, and reflective cracking of the asphalt layer. Cracking in asphaltic pavement layers causes primary failure of the roadway structure and leads to long-term durability issues that are often related to moisture damage. The fracture resistance and characteristics of asphalt materials significantly influence the service life of asphalt pavements and, consequently, the maintenance and management of the pavement network. In spite of the significance, proper characterization of the fracture process and fundamental fracture properties of the asphaltic materials have not been adopted in the current pavement design-analysis procedures, which are generally phenomenological.

Cracking is probably the most challenging issue to predict and control. This is because of the complex geometric characteristics and inelastic mechanical behavior of the asphalt mixtures, which are temperature sensitive and rate dependent. These characteristics make any solution to the cracking problem in asphalt mixtures almost impossible to achieve with the aid of the theory of linear elastic fracture mechanics (LEFM). LEFM is only able to predict the stress state close to the crack tips of damaged bodies if the fracture process zone (FPZ) around the crack tip is very small. The FPZ in asphaltic materials might be large, as typical quasi-brittle materials are [1].

Some studies have evaluated the fracture toughness of asphalt mixtures using the J-integral concept or the stress intensity approach [2–4]. Others have conducted fracture tests and numerical analyses by means of a cohesive-zone model to study the fracture behavior of asphalt mixtures [5–8]. The cohesive-zone modeling approach has recently received increased attention from the asphaltic materials and pavement mechanics community to model crack initiation and growth. This is because the cohesive-zone approach can properly model both brittle and ductile fracture, which is frequently observed in asphaltic roadways because of the wide range of service temperatures and traffic speeds. Moreover, it can provide an efficient tool that can be easily implemented in various computational methods, such as finite-element and discrete-element methods, so that fracture events in extremely complicated mixture microstructure can also be simulated.

Most of the fracture tests have usually used conventional extensometers or clip-on gauges that are far from the actual FPZ to monitor averaged deformations or displacements of specimens for the characterization of fracture properties of asphalt mixtures. However, the true fracture properties of asphalt mixtures could be misled by as much as an order of magnitude because the material responses captured by the extensometers or clip-on gauges are

Manuscript received November 22, 2011; accepted for publication August 30, 2012; published online January 22, 2013.

[1]Ph.D. Candidate, Dept. of Civil Engineering, 362D Whittier Research Center, Univ. of Nebraska, Lincoln, NE 68583, e-mail: sooim@huskers.unl.edu

[2]Associate Professor, Dept. of Civil Engineering, 224 Engineering Building, Kyung Hee Univ., Yongin-si, Gyeonggi-do 446-701, South Korea (Corresponding author), e-mail: ykim3@khu.ac.kr

[3]Post-doctoral Research Associate, Dept. of Civil Engineering, 362H Whittier Research Center, Univ. of Nebraska, Lincoln, NE 68583, e-mail: hban2@unlnotes.unl.edu

TABLE 1—*Gradation and properties of aggregates used.*

Sieve analysis (wash) for gradation										
Aggregate sources	19 mm	12.7 mm	9.5 mm	#4	#8	#16	#30	#50	#100	#200
16-mm limestone	100	95	89	–	–	–	–	–	–	–
6.4-mm limestone	100	100	100	72	–	–	–	–	–	–
Screenings	100	100	100	100	36	21	14	10	7	3.5
Combined gradation	100	95	89	72	36	21	14	10	7	3.5
Physical and geometrical properties										
Combined properties	$G_{sb} = 2.577$, FAA(%) = 45.0, CAA (%) = 89.0, F&E (%) = 0.0									

limited to accurately represent material behavior at the actual FPZ. This discrepancy can become worse if the material is highly heterogeneous and inelastic [9,10], which is typical in asphaltic paving materials. In addition, most of the studies have adopted low-temperature testing conditions in which the type of fracture is much more brittle than it should be to accurately characterize fracture behavior such as fatigue cracking observed at intermediate service temperatures.

A better understanding of FPZ at realistic service conditions is considered a critical step to the development of mechanistic design-analysis procedures for asphaltic mixtures and pavement structures. This is because the characteristics of the FPZ represent the true material behavior related to the fracture damage, which consequently leads to the selection of proper testing methods and modeling-analysis techniques that are appropriate to address the complex local fracture process. However, such careful efforts to characterize the FPZ in asphalt concrete mixtures have not yet sufficiently been made. To the authors' best knowledge, only limited attempts [10–13] have been carried out because of many experimental–analytical complexities.

Study Objectives and Scope

This study presents experimental efforts and numerical simulations to characterize the FPZ and fracture properties of typical asphaltic paving mixtures subjected to various loading rates at different temperatures. To that end, two laboratory tests—uniaxial compressive cyclic tests to identify the linear viscoelastic properties and semi-circular bending (SCB) fracture tests to characterize the fracture properties—of a dense-graded asphalt concrete mixture are conducted at various loading rates and testing temperatures. The SCB fracture test is also incorporated with a digital image correlation (DIC) system and the finite-element model simulations, including material viscoelasticity and cohesive-zone fracture to effectively capture local fracture processes. The specific objectives of this paper are as follows:

- To explore a testing program that can characterize fracture behavior at the FPZ of asphaltic paving materials;
- To identify fracture properties of the asphalt mixture at a wide range of loading rates (i.e., 1, 5, 10, and 50 mm/min) and service temperatures (i.e., −10, 0, 21, and 30°C); and
- To seek better insights into the temperature-sensitive and rate-dependent fracture behavior of the asphaltic paving mixtures, which is to eventually advance the current pavement-design practices.

Materials and Mixture

For the fabrication and testing of the dense-graded asphalt mixture, three aggregates were selected and blended: 16-mm limestone, 6.4-mm limestone, and screenings. All three aggregates are limestone with the same mineralogical origin. The nominal maximum aggregate size (NMAS) of the final aggregate blend was 12.5 mm. Table 1 illustrates gradation, bulk specific gravity (G_{sb}), and consensus properties [i.e., fine aggregate angularity (FAA), coarse aggregate angularity (CAA), flat and elongated (F&E) particles] of the aggregates used in this study. The asphalt binder used in this study was Superpave performance graded binder PG 64-28. With the limestone aggregate blend and the binder, volumetric design of the mixture was performed; this resulted in a binder content of 6.0 % by weight of the total mixture to meet the 4.0 % target air voids and other necessary volumetric requirements.

Experimental Program

Figure 1 briefly illustrates the process of sample fabrication and laboratory tests performed for this study. Laboratory tests were conducted to obtain linear viscoelastic properties and to characterize the fracture properties of the mixture. As shown, cylindrical mixture samples were fabricated using a Superpave gyratory compactor (SGC). Two different specimen geometries were extracted from the SGC samples: (a) cylindrical cores (150 mm in height and 100 mm in diameter) to be used for determining the linear viscoelastic properties of the mixture, and (b) semi-circular bending (SCB) specimens (150 mm in diameter and 25 mm thick, with a 2.5-mm-wide and 25-mm-deep mechanical notch) to be used for fracture tests of the mixture.

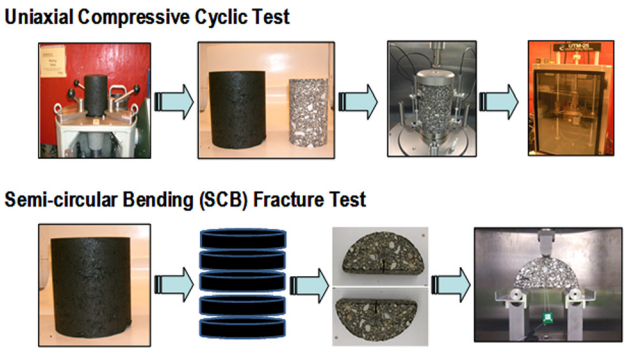

FIG. 1—*Specimen fabrication and laboratory tests performed for this study.*

Uniaxial Compressive Cyclic Tests for Linear Viscoelastic Properties

Uniaxial compressive cyclic tests were performed for the linear viscoelastic stiffness of the mixture. The loading levels were carefully adjusted until the strain levels were within the range of 0.00005–0.000075. Three linear variable differential transformers (LVDTs) were mounted onto the surface of the specimen at 120° radial intervals with a 100-mm gauge length. As suggested in the AASHTO TP62 [14], five temperatures (−10, 4.4, 21.1, 37.8, and 54.4°C) and six loading frequencies (25, 10, 5, 1.0, 0.5, and 0.1 Hz) were used, and the frequency–temperature superposition concept was applied to obtain the linear viscoelastic master curves of the storage modulus in the frequency domain for a target reference temperature. The testing results of the storage modulus as a function of angular frequency were then fitted with a mathematical function (i.e., Prony series) based on the generalized Maxwell model as follows:

$$E'(\omega) = E_\infty + \sum_{i=1}^{n} \frac{E_i \omega^2 \rho_i^2}{\omega^2 \rho_i^2 + 1} \tag{1}$$

where:

$E'(\omega)$ = storage modulus,
ω = angular frequency,
E_∞ = long-time equilibrium modulus,
E_i = spring constants in the generalized Maxwell model,
ρ_i = relaxation time, and
n = number of Maxwell units in the generalized Maxwell model.

If the storage moduli at a reference temperature T_o are known, the storage moduli at any given arbitrary temperature T can be obtained by using a frequency–temperature shift factor a_T as follows:

$$a_T = \frac{\omega_{T_o}}{\omega_T} \tag{2}$$

Using the Prony series parameters (E_∞, E_i, and ρ_i) obtained by fitting the experimental data with storage modulus, the relaxation modulus can be expressed in the time domain as follows:

$$E(t) = E_\infty + \sum_{i=1}^{n} E_i e^{-\frac{t}{\rho_i}} \tag{3}$$

where:

$E(t)$ = relaxation modulus in time domain and
t = loading time.

SCB Tests for Fracture Properties

To characterize the fracture properties of asphalt mixtures, four geometries have typically been pursued by researchers in the asphaltic materials and pavement mechanics field. These are: (i) single-edge notched beam, SE(B), specimen [2,15,16]; (ii) disc-shaped compact tension, DC(T), specimen [17–19]; (iii) semi-circular bending, SCB, specimen [11,20–23]; and (iv) double-edged notched tension, DENT, specimen [12]. Among the various options, SCB testing was selected in this study because it has several benefits compared to other fracture test methods. Even if it has some limitations [18], SCB testing is practically attractive in that it is very repeatable, simple to perform, and that multiple testing specimens can be easily prepared through a routine process of mixing and Superpave gyratory compacting of asphalt mixtures. Furthermore, the SCB geometry is even more attractive considering the fracture characteristics of field cores, which are usually circular. Based on these practical benefits, the SCB testing configuration has become a popular geometry for evaluating the fracture behavior of bituminous mixtures.

Before testing, individual SCB specimens were placed inside the environmental chamber of a mechanical testing machine for temperature equilibrium targeting the four different testing temperatures (−10, 0, 21, and 30°C). Following the temperature conditioning step, specimens were subjected to a simple three-point bending configuration with four different monotonic displacement rates (1, 5, 10, and 50 mm/min) applied to the top center line of the SCB specimens at each testing temperature. Metallic rollers separated by a distance of 122 mm (14 mm from the edges of the specimen) were used to support the specimen. Reaction force at the loading point and vertical crosshead displacements were monitored by the data-acquisition system installed in the mechanical testing machine.

As mentioned earlier, the SCB fracture test was incorporated with the DIC system to effectively capture time-dependent deformations, such as the local fracture process of the mixture during testing. The DIC recognizes the surface structure of the specimen in digital video images and allocates coordinates to the image pixels. The first image represents the undeformed state, and further images are recorded during the deformation of the specimen. Then, the DIC compares the digital images and calculates the displacement and deformation of the specimen. To facilitate the DIC process more efficiently, the specimen was painted in white and then was stamped to create numerous black dots on the white background. The black dots act as material points for the full-field deformation characteristics such as formation and movement of the FPZ as cracks grow because of loading. Two pairs of dot gauges were additionally attached to the surface of the specimen to more accurately capture the opening displacements at the mouth (denoted as notch mouth opening displacements, NMOD) and at the tip (denoted as notch tip opening displacements, NTOD) of the initial notch. Moreover, vertical displacements at a material point close to the loading zone were also monitored by DIC to provide load point displacements (LPD). A clip-on gauge was also used to capture the NMOD to compare measurements from DIC. The DIC system used in this study incorporated a high-speed video camera that can accurately monitor specimen deformation in strains from 0.05 % up to 500 %. Figure 2 shows the SCB testing setup, black dot image pattern and the additional two-pair gauge points attached on the specimen surface for DIC analysis, and the clip-on gauge installed at the bottom of the specimen.

Uniaxial Compressive Cyclic Test Results

A total of four replicates were tested and values of storage modulus at each different testing temperature over the range of loading frequencies were obtained. The test results from replicates were then averaged to produce 30 individual storage moduli at all levels of temperature and frequency to produce a stiffness master curve

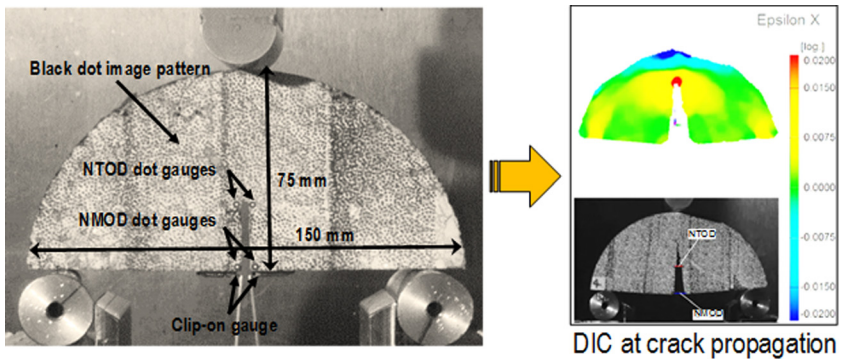

FIG. 2—*SCB fracture testing setup incorporated with DIC used in this study.*

constructed at a reference temperature. Figure 3 exemplifies master curves of four replicates and their average at a reference temperature of 21°C. The test results among the replicates were generally repeatable without large discrepancies.

The reference temperature is −10, 0, 21, or 30°C for this study, because they are the temperatures used to conduct the SCB fracture tests, which are simulated through the finite-element model to characterize local fracture properties of the mixture as discussed in later sections. The master curve represents the stiffness of the mixture in a wide range of loading frequencies (or loading times, equivalently). Master curves are constructed using the frequency (or time)–temperature superposition by shifting data at various temperatures with respect to loading frequency until the curves merge into a single smooth function. After the shifting is completed, the master curve at an arbitrary reference temperature was then fitted with the Prony series (shown in Eq 1) to determine linear viscoelastic material parameters. Table 2 presents shift factors and Prony series parameters determined for each different target temperature.

SCB Fracture Test Results and Discussion

A total of 48 SCB specimens were prepared to complete three replicates per test case of the 16 test cases in total (four loading rates at four temperatures). Figure 4 exemplifies the SCB test results

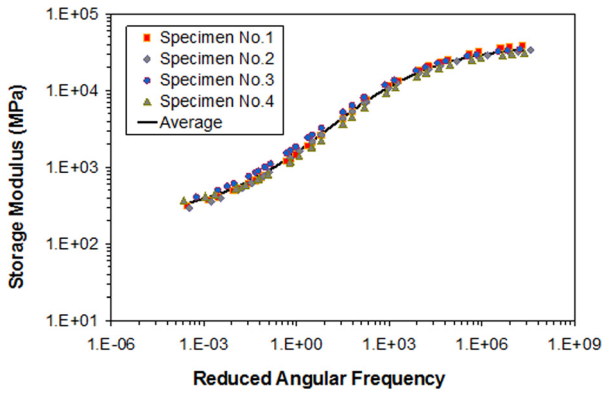

FIG. 3—*Uniaxial compressive cyclic test results at a reference temperature of 21°C.*

from a test case at 5 mm/min and 30°C and a test case at 50 mm/min. and −10°C by plotting the reaction forces at the point of load application as the opening displacements increased. As presented in the figure, the test results among the replicates at the same testing conditions were generally repeatable without large discrepancies. The coefficient of variation in the peak force from each testing case was between 2.6 % and 19.2 %.

In an attempt to illustrate the effects of testing conditions on the mixture's fracture behavior, Fig. 5 presents the SCB test results by plotting the average values between the reaction forces and opening displacements at different loading rates by the different testing temperatures [i.e., 5(*a*) for −10°C, 5(*b*) for 0°C, 5(*c*) for 21°C, and 5(*d*) for 30°C]. Clearly, the figure reveals the temperature-related global mechanical behavior of the asphalt mixture. At −10°C, although the peak force slightly increases as the loading rate becomes higher, it appears that the fracture behavior is relatively rate independent, which is typically observed from a linear elastic fracture state. However, the rate-dependent behavior is obvious and becomes more evident when the testing temperature is higher. Slower loading speeds produce more compliant responses than faster cases. Loading rates clearly affect both the peak force and the material softening, which is represented by the shape of the post-peak tailing. The trends presented in Fig. 5 suggest that the rate- and temperature-dependent nature of the fracture characteristics needs to be considered when modeling the mechanical performance of typical asphalt mixtures and pavements with which a wide range of strain rates and service temperatures is usually associated.

As mentioned earlier, to measure various deformation characteristics simultaneously, the DIC was incorporated in this study with two other displacements measuring methods: (i) a clip-on gauge attached to capture the NMOD, and (ii) crosshead displacements to provide vertical LPD. This is to evaluate any differences and/or compatibility between the two strain-measuring approaches: the conventional gauge method and the DIC technique. Furthermore, as discussed below in the section Fracture-Energy Characterization, fracture energy can be estimated by several different measurements and analysis approaches. Any similarities and/or compatibility between different fracture-energy values estimated from different measurements and approaches can be examined.

Figure 6 shows the force–displacement curves of specimen No. 3 in Fig. 4. It plots the opening displacements measured from

TABLE 2—*Prony series parameters determined for each different reference temperature.*

Reference Temperature	−10°C		0°C		21°C		30°C	
Prony Series Parameters	E_i (MPa)	ρ_i (s)	E_i (MPa)	ρ_i (s)	E_i (MPa)	ρ_i (s)	E_i (MPa)	ρ_i (s)
1	7391.7	1.0×10^{0}	8095.7	1.0×10^{-1}	9095.4	1.0×10^{-5}	9028.5	1.0×10^{-5}
2	5931.0	1.0×10^{1}	5312.2	1.0×10^{0}	6778.9	1.0×10^{-4}	4721.3	1.0×10^{-4}
3	6561.0	1.0×10^{2}	4754.5	1.0×10^{1}	7001.4	1.0×10^{-3}	4216.1	1.0×10^{-3}
4	4526.6	1.0×10^{3}	2243.3	1.0×10^{2}	4250.9	1.0×10^{-2}	1879.0	1.0×10^{-2}
5	2679.8	1.0×10^{4}	1089.9	1.0×10^{3}	2286.2	1.0×10^{-1}	999.9	1.0×10^{-1}
6	1238.2	1.0×10^{5}	423.5	1.0×10^{4}	962.4	1.0×10^{0}	397.9	1.0×10^{0}
7	566.9	1.0×10^{6}	203.6	1.0×10^{5}	430.7	1.0×10^{1}	205.7	1.0×10^{1}
8	252.6	1.0×10^{7}	89.8	1.0×10^{6}	186.8	1.0×10^{2}	93.2	1.0×10^{2}
9	124.1	1.0×10^{8}	47.3	1.0×10^{7}	92.8	1.0×10^{3}	52.0	1.0×10^{3}
10	61.0	1.0×10^{9}	23.5	1.0×10^{8}	45.3	1.0×10^{4}	26.2	1.0×10^{4}
11	72.6	1.0×10^{10}	9.1	1.0×10^{9}	53.8	1.0×10^{5}	34.0	1.0×10^{5}
∞	236.1	–	323.7	–	215.3	–	229.5	–
Shift factor log a_T	5.26		2.44		0		−1.25	

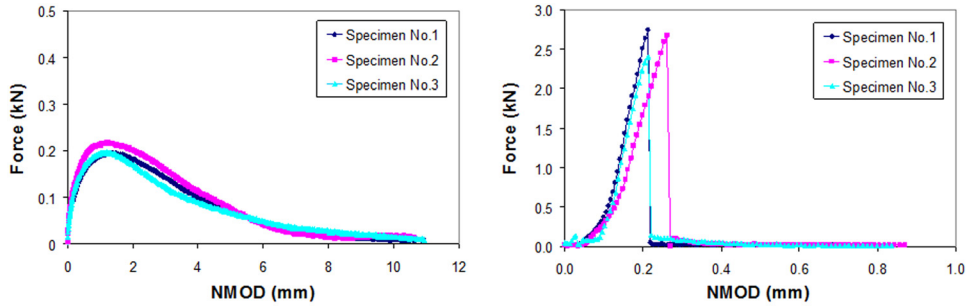

FIG. 4—*SCB test results (force–NMOD): (a) at 5 mm/min and 30° C, and (b) at 50 mm/min and −10° C.*

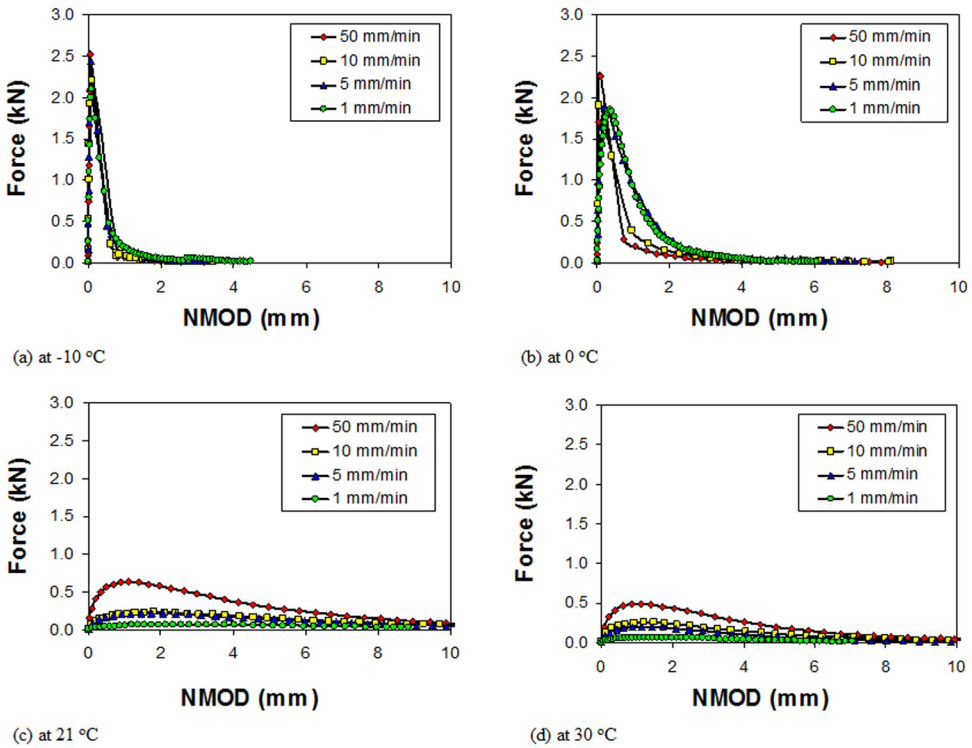

FIG. 5—*SCB test results (force–NMOD) at different loading rates and testing temperature.*

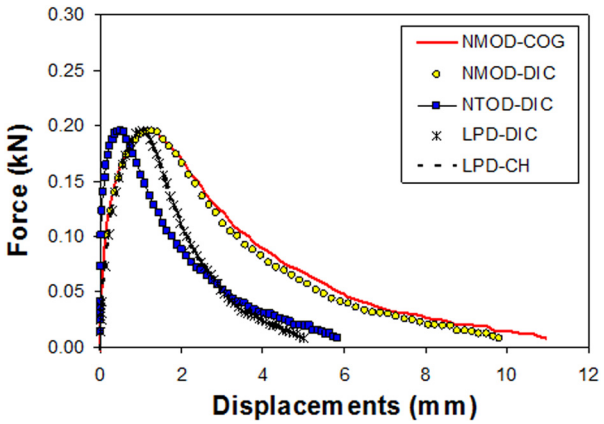

FIG. 6—*Force versus displacements measured using different methods.*

the DIC (i.e., NMOD-DIC and NTOD-DIC), opening displacements captured by the clip-on gauge (i.e., NMOD-COG), and load point displacements measured by the DIC (i.e., LPD-DIC), and cross-head (i.e., LPD-CH). As shown, the DIC results agree well with these measurements. From the result, it can be inferred that DIC measurements (both NMOD-DIC and LPD-DIC) are quite compatible with measurements obtained from the clip-on gauge (NMOD-COG) and the cross-head (LPD-CH) throughout the SCB fracture test. This seems to be an attractive finding for practical reasons, because the DIC process is time-consuming, expensive, and requires additional techniques for data analysis compared to the use of the conventional displacement measuring systems. In contrast, it is also obvious that DIC is preferred to investigate the deformation characteristics of time-dependent, heterogeneous media, such as asphalt mixtures, because it is versatile in terms of providing detailed information on both full-field surface displacements and local material behavior. This feature is particularly important for fracture investigation, because fracture is local behavior that needs to be characterized with local measurements such as the NTOD.

Figure 7 presents visual observation of SCB specimens after testing at the four different temperatures. The cracking pattern is presented in 7(*a*), and the fracture surfaces of individual specimens are shown in 7(*b*). It appears that cracks propagated straight from the crack tip and traveled through aggregates at low temperatures, whereas the crack trajectory was significantly affected by the mixture microstructure at ambient temperatures (21°C and 30°C). As expected, the fracture process at ambient temperatures without moisture damage occurred within the black matrix phase, which resulted in a deflected crack path around coarse aggregates and the black fracture surface, as demonstrated in the figure.

Fracture-Energy Characterization

Using SCB test results, the average fracture energy was obtained for each test case. There were several methods [10,18,23–25] found in the open literature to calculate the fracture energy. Among them, this study attempted two approaches: one is based on the concept of the critical energy release rate and the other is by modeling the SCB fracture tests with cohesive-zone elements. The first approach is relatively simple to characterize the fracture energy by merely calculating an area under the load–displacement curve that is normalized by the area of the fractured surface, i.e., the initial ligament length multiplied by the specimen thickness. However, the fracture energies obtained from the first approach may mislead true fracture characteristics of the material, because the force–displacement curves are global measurements that are dependent on the choice of displacement measurements, testing specimen geometry and applied boundary conditions. Furthermore, the viscoelastic nature of the asphaltic material creates a further complication in identifying fracture properties. Some parts of the total energy monitored by calculating the area below the

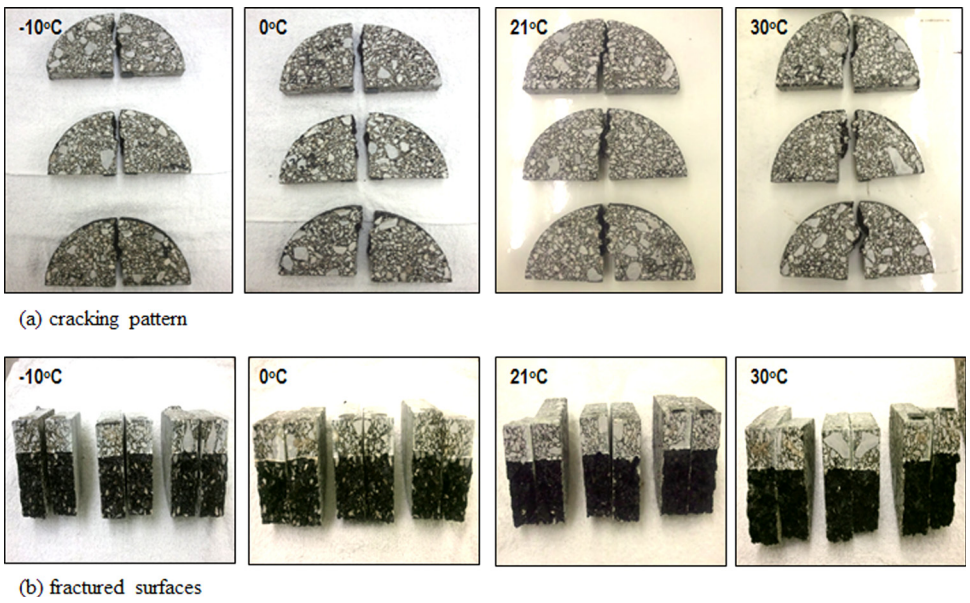

FIG. 7—*Visual observation of SCB specimens after testing.*

TABLE 3—*Summary of average fracture energy (J/m^2) and COV (%).*

		From Clip-On Gage		From Cross-Head		From DIC					
		Force–NMOD		Force–LPD		Force–NTOD		Force–NMOD		Force–LPD	
Temperature (°C)	Rates (mm /min)	Mean (J/m^2)	COV (%)	Mean (J/m^2)	COV (%)	Mean (J/m^2)	COV (%)	Mean (J/m^2)	COV (%)	Mean (J/m^2)	COV (%)
−10	1	787.1	25.6	453.5	26.4			DIC was not used			
	5	808.6	2.8	406.8	19.6	564.8	0.5	813.2	0.8	390.7	0.1
	10	767.0	15.3	393.2	26.2			DIC was not used			
	50	770.7	16.7	370.7	7.3			DIC was not used			
0	1	1750.2	15.6	1076.7	12.0			DIC was not used			
	5	1789.4	30.8	1080.5	30.2	1117.2	32.4	1779.2	34.0	N/A	
	10	1169.4	5.4	690.4	7.3			DIC was not used			
	50	980.4	8.1	531.4	4.4			DIC was not used			
21	1	395.9	17.4	186.2	16.6	240.7	25.4	413.1	24.6	190.5	20.3
	5	1082.2	11.1	539.5	9.2	551.8	7.7	1043.1	14.5	525.5	11.3
	10	1200.6	8.4	636.4	10.6	555.6	10.1	1112.0	1.5	618.3	5.0
	50	2670.5	4.1	1462.3	4.0	1468.4	6.7	2624.1	2.4	1421.5	2.8
30	1	216.6	13.3	111.8	15.5	114.0	15.9	209.6	14.4	113.4	18.4
	5	664.5	4.8	335.4	4.0	379.1	10.3	651.1	5.7	357.3	4.0
	10	1025.7	19.5	536.4	20.2	574.7	26.4	1021.8	21.6	521.6	13.5
	50	1851.3	11.8	967.9	17.0	1081.3	13.8	1798.5	15.8	927.0	14.6

force–displacement curves are related to the energy dissipated because of material viscoelasticity. Fracture characteristics along the fracture process zone should be examined locally, not by the global force–displacement test results. Based on this fact, the second approach, finite-element simulations of the SCB tests with cohesive-zone model, were conducted to determine the fracture properties that are locally associated to initiate and propagate cracks through the specimens.

Fracture Energy from Force–Displacement Curve

For comparison purposes, the fracture energy was calculated using the five different sets of load–displacement data: force–NMOD-DIC, force–NTOD-DIC, force–LPD-DIC, force–NMOD-COG, and force–LPD-CH. Table 3 summarizes the average fracture energy and its sample-to-sample variation, which is represented by the coefficient of variation (COV), of each test case from the five different displacement measurements.

Most test cases showed low COV values, usually less than 20 %, from three replicates; exceptions were some cases where relatively high COV values up to 30 % were determined. The COV values obtained in this study were in a similar range, between 15 % and 34 %, to those found in a recent study that investigated the low-temperature fracture characteristics of asphalt concrete mixtures using the SCB geometry [25].

As exemplified in Fig. 6, and as Table 3 confirms, fracture energies obtained from DIC data (NMOD-DIC and LPD-DIC) are very similar to the fracture energies estimated, respectively, by the clip-on gauge measurements (NMOD-COG) and the cross-head displacements (LPD-CH), regardless of loading rates and testing temperatures.

Moreover, as previously observed in Fig. 6, the fracture-energy values obtained from force–NMOD curves were always greater than those from the force–NTOD curves. This is because the tip opening displacements are naturally smaller than the mouth opening displacements when the specimen is subjected to a bending mode fracture such as SCB. Because the fracture process is locally initiated at the notch tip, the fracture energy characterized using NTOD data is more representative than the value obtained from the NMOD measurements. The fracture energy estimated from NMOD data clearly overestimates the true material fracture toughness, and the deviation in the fracture energy between the NTOD and NMOD measurements becomes greater as temperature increases. At −10°C, the fracture energy from force–NTOD curves was about 30 % less than that from force–NMOD curves, whereas the level of deviation increased to 37 % at 0°C and up to 50 % at 21°C and 30°C depending on the loading rate. A similar finding was also observed in other studies [10,23]. This clearly indicates that, although it has been widely adopted because of its simple and practical aspects, the use of NMOD measurements in the fracture characterization of asphaltic materials needs great care and is even more cautious at elevated temperatures when the materials present several sources of energy dissipation, such as material viscoelasticity/plasticity and crack growth.

Another interesting observation from the table is that average fracture energies calculated from the LPD data are smaller than, but similar to the fracture-energy values estimated from the NTOD data, although the LPD measurements have nothing to do with the local fracture process. This seems to be an attractive observation for practical purposes, because the LPD measurements from the SCB test are easy to take by simply monitoring vertical displacements (for instance the cross-head movements), whereas

the NTOD data are relatively hard to obtain because it needs special measuring devices such as the video cameras and DIC system as pursued in this study.

Fracture Energy from Finite-Element Modeling with Cohesive Zone

The FPZ is a nonlinear zone characterized by progressive softening, for which the stress decreases at increasing deformation. The nonlinear softening zone is surrounded by a non-softening nonlinear zone, which represents material inelasticity. Bazant and Planas [1] skillfully classified the fracture process behavior in certain materials into three types: brittle, ductile, and quasi-brittle. Each type presents different relative sizes of those two nonlinear zones (i.e., softening and non-softening nonlinear zones). Figure 8 presents the third type of behavior, so-called quasi-brittle fracture. It includes situations in which a major part of the nonlinear zone undergoes progressive damage with material softening caused by microcracking, void formation, interface breakages, frictional slips, and others. The softening zone is then surrounded by the inelastic material yielding zone, which is much smaller than the softening zone. This behavior includes a relatively large FPZ, as shown in the figure. Asphaltic paving mixtures are usually classified as quasi-brittle materials [1,26,27].

The FPZ can be modeled in many different ways, and one of the well-known approaches is to use a cohesive zone. At the crack tip, the cohesive-zone constitutive behavior reflects the change in the cohesive-zone material properties because of microscopic damage accumulation ahead of the crack tip. This behavior can be expressed by the general traction–displacement cohesive-zone relationship as follows:

$$T_i(x_m, t) = T_i\{\Delta_i(x_m, \tau)\} \tag{4}$$

where:

T_i = cohesive-zone traction (T_n for normal and T_t for tangential traction),

Δ_i = cohesive-zone displacement (Δ_n for normal and Δ_t for tangential displacement),

x_m = spatial coordinates, and

t = time of interest.

Cohesive-zone models regard fracture as a gradual phenomenon in which separation (Δ) takes place across an extended crack tip (or cohesive zone) and where fracture is resisted by cohesive tractions (T). The cohesive zone effectively describes the material resistance when material elements are being displaced. Equations relating normal and tangential displacement jumps across the cohesive surfaces with the proper tractions define a cohesive-zone model. Among numerous cohesive-zone models developed for different specific purposes, this study used an intrinsic bilinear cohesive-zone model [6,28,29]. As shown in Fig. 8, the model assumes that there is a recoverable linear elastic behavior until the traction (T) reaches a peak value, or cohesive strength (T_{max}) at a corresponding separation in the traction–separation curve. At that point, a nondimensional displacement (λ) can be identified and used to adjust the initial slope in the recoverable linear elastic part of the cohesive law. This capability of the bilinear model to adjust the initial slope is significant because it can alleviate the artificial compliance inherent to intrinsic cohesive-zone models. The λ value has been determined through a convergence study designed to find a sufficiently small value to guarantee a level of initial stiffness that renders insignificant artificial compliance of the cohesive-zone model. It was observed that a numerical convergence can be met when the effective displacement is smaller than 0.0005 [30], which has been used for simulations in this study. Upon damage initiation, T varies from T_{max} to 0, when a critical displacement (δ_c) is reached and the faces of the cohesive element are fully and irreversibly separated. The cohesive-zone fracture energy (Γ_c), which is the locally estimated fracture toughness, can then be calculated by computing the area below the bilinear traction–separation curve with peak traction (T_{max})and critical displacement (δ_c) as follows:

$$\Gamma_c = \frac{1}{2}\delta_c T_{max} \tag{5}$$

Figure 9 presents a finite-element mesh, which was finally chosen after conducting a mesh convergence study [30]. The specimen was discretized using two-dimensional (plane stress), three-node triangular linear elements for the bulk specimen and zero thickness, four-node cohesive-zone elements were inserted along the center of the mesh to permit mode I crack growth in the simulation of SCB testing. The Prony series parameters (shown in Table 2) determined from the uniaxial compressive cyclic tests were used and a constant Poisson's ratio of 0.35 was assumed for the viscoelastic elements, and the bilinear cohesive-zone model illustrated in Fig. 8 was used to simulate fracture in the middle of the SCB specimen as the opening displacements increased. It should be noted that the simulation conducted herein involves several limitations at this stage by assuming the mixture as homogeneous and isotropic with only mode I crack growth, which may not represent the true fracture process of specimens particularly tested at the ambient temperatures where mixture heterogeneity

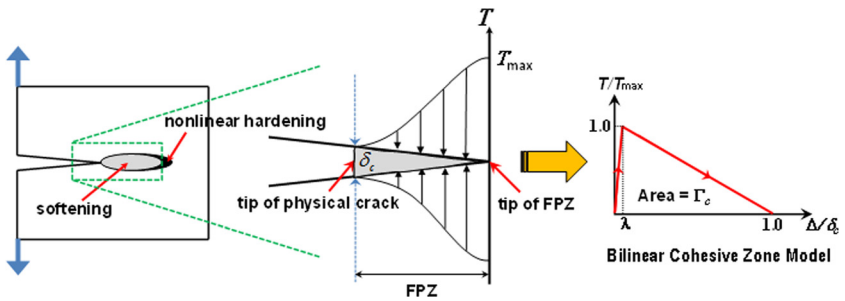

FIG. 8—*Schematic illustration of FPZ of typical quasi-brittle materials.*

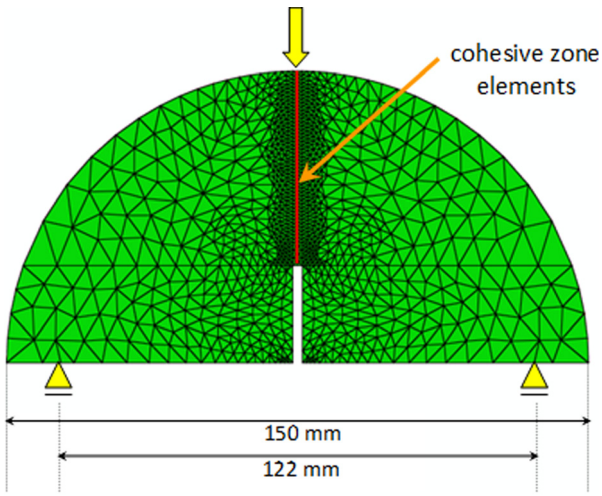

FIG. 9—*A finite-element mesh constructed after convergence study to model the SCB testing.*

(i.e., microstructural characteristics) and mixed-mode fracture is not trivial as demonstrated in Fig. 7.

The cohesive-zone fracture properties (two independent values of the three: T_{max}, δ_c, and Γ_c) in the bilinear model were determined for each case through the calibration process until a good match between test results and numerical simulations was observed. Figure 10 presents a strong agreement between the test results (average of the three SCB specimens) and finite-element simulations. Resulting fracture properties (T_{max} and Γ_c) at each different loading rate and testing temperature are presented in Table 4.

Discussion of Test-Analysis Results

In an attempt to further investigate the fracture characteristics of asphalt mixtures when they are subjected to different loading rates, different temperatures, and analysis methods, Fig. 11 was produced using fracture-energy values from the force–NMOD-COG curves, force–NTOD-DIC curves, and cohesive-zone modeling at different loading rates and temperatures. The fracture energy obtained at −10°C does not seem to be affected by the loading rate, whereas the fracture energies at 0°C to 30°C clearly change as the loading rates vary. The negligible rate-dependency at −10°C is considered reasonable because the mixture at low-temperature conditions, such as −10°C, is in the linear elastic fracture domain, where the rate-dependent fracture characteristics of viscoelastic materials usually disappear. As temperature increases to 0°C, the mixture becomes viscoelastic so that it can dissipate more energy to fracture. Therefore, the magnitude of fracture energy at 0°C is greater than the fracture energy at −10°C over all the loading rates applied in this study. Regarding the trend of fracture energy to the loading rate, it decreases as the loading speed is faster, which agrees with observations in other studies [18,25]. At ambient temperatures (21°C and 30°C), the rate-dependent fracture behavior is obvious, and the fracture energy increases as the loading rates become higher. The trend is in accordance with what has been reported in several studies that have attempted to characterize the rate-related fracture behavior of adhesive and polymeric materials [31–33]. In those studies, fracture energy tends to be constant when cracks propagate at lower speeds, whereas it increases with crack velocity for an intermediate level of crack velocity.

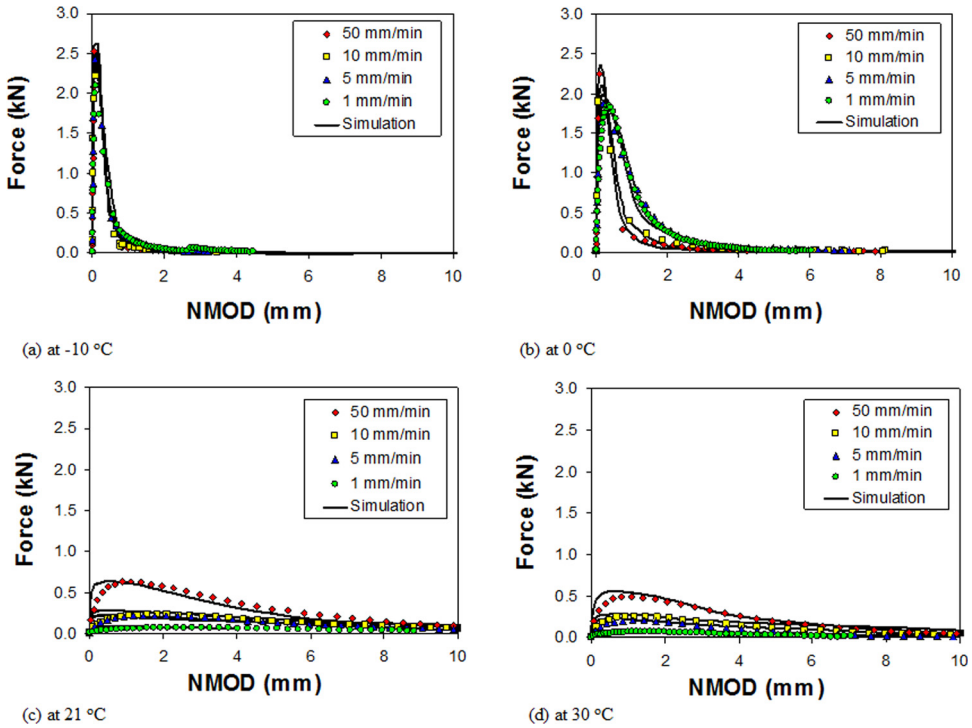

FIG. 10—*SCB test results versus cohesive-zone model simulation results.*

TABLE 4—*Cohesive-zone fracture parameters determined.*

Temperature (°C)	Loading Rate (mm/min)	Cohesive-Zone Fracture Parameters T_{max} (kPa)	Γ_c (J/m^2)
−10	1	3.2×10^3	350
	5	3.4×10^3	350
	10	3.6×10^3	350
	50	4.0×10^3	350
0	1	2.7×10^3	750
	5	2.7×10^3	700
	10	3.2×10^3	450
	50	3.6×10^3	400
21	1	9.0×10^1	250
	5	2.5×10^2	500
	10	3.0×10^2	700
	50	7.0×10^2	1200
30	1	8.0×10^1	220
	5	2.5×10^2	400
	10	3.2×10^2	550
	50	6.5×10^2	900

Regarding the fracture characteristics by different approaches, Fig. 11 shows that the fracture energies obtained from the area under the force–NMOD (or force–NTOD) curve are always larger than the fracture energy identified from the cohesive-zone modeling, and the deviation between the two approaches usually decreases as the loading rates are higher. Furthermore, it is clear that fracture-energy values obtained from the force–NTOD curve are closer to the values characterized at the local FPZ through the cohesive-zone modeling than those obtained from the force–-NMOD curve. This observation was expected because, as noted previously, the energy obtained from NMOD measurements overestimates the true fracture toughness.

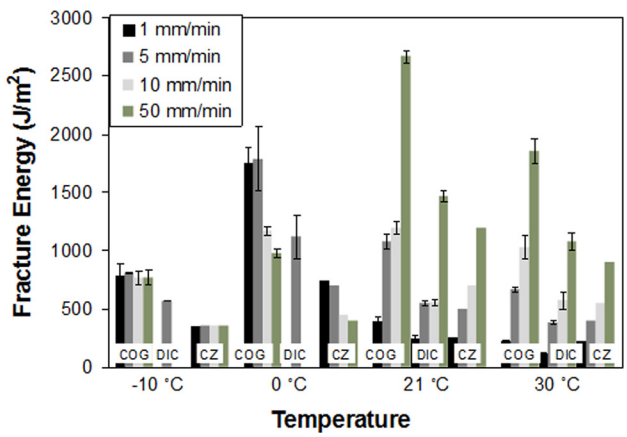

FIG. 11—*Comparison of fracture energies.*

Concluding Remarks

This study presented experimental-numerical efforts to characterize the FPZ and fracture property of typical asphaltic paving mixtures. To do that, two laboratory tests—uniaxial compressive cyclic tests to identify the linear viscoelastic properties and semi-circular bending (SCB) fracture tests to characterize the fracture properties—of a dense-graded asphalt concrete mixture were conducted at various loading rates and testing temperatures. The SCB fracture test was also incorporated with the DIC system and the finite-element model simulations including material viscoelasticity and cohesive-zone fracture to effectively capture local fracture processes. Based on the results and findings, the following conclusions can be made.

- The SCB fracture test presented reasonable and repeatable results. The coefficient of variation between replicates was acceptable, and the test was successfully suited to various strain measuring systems. Fracture behavior at the process zone presented sensitive responses to the loading rates and testing temperatures.
- The DIC results (NMOD and LPD) were quite compatible with conventional measurements obtained from the clip-on gauge and the cross-head. The DIC could also provide full-field surface displacements and local fracture process. This feature was not quite intensively used for this study at this time, but can be used to more accurately characterize the time-varying local FPZ of the mixture as some recent studies [34,35] attempted for different materials.
- The fracture energies obtained from force–NMOD (or force–NTOD) curves were always greater than those from the cohesive-zone modeling. The deviation in the fracture energy between the two approaches was greater as the temperature increased and loading rates were lower. This indicates that fracture process is a local phenomenon that needs to be identified at the tip of FPZ. The fracture characteristics obtained from NMOD measurements overestimate the true fracture toughness, as it includes other sources of energy dissipation, such as material viscoelasticity, which is not related to the fracture process.
- At low temperatures, such as −10°C, the fracture process was not rate-dependent, whereas the fracture energy at 0°C to 30°C clearly presented rate-related behavior. Fracture energy dropped as the loading speed became faster at 0°C; however, the trend was the opposite at ambient temperatures. The findings from this study remains further investigation to explain relevant mechanisms which seem to be related to the material's response at intermediate temperatures (and at slower loading rates) where plastic and/or viscoplastic behavior may be significant. The non-viscoelastic material behavior has not been considered in this study.
- The test and analysis results in this paper suggest that the rate- and temperature-dependent fracture properties are necessary in the structural design of asphaltic pavements with which a wide range of strain rates and service temperatures is usually associated.

Acknowledgments

The writers appreciate the financial support from the Nebraska Department of Roads in US and MKE (Ministry of Knowledge Economy) - ISTK (Korea Research Council for Industrial Science and Technology) of Republic of Korea (Grant: Production of Synthetic Crude Oils/Petrochemicals by Upgrading Package Process of Low-Cost Heavy Oil Fractions). The BM3 Laboratory in College of Engineering at the University of Nebraska is also gratefully acknowledged for the DIC system.

References

[1] Bazant, Z. P. and Planas, J., *Fracture and Size Effect in Concrete and Other Quasibrittle Materials*, CRC Press, Boca Raton, 1998.

[2] Mobasher, B., Mamlouk, M. S., and Lin, H. M., "Evaluation of Crack Propagation Properties of Asphalt Mixtures," *J. Transport. Eng.*, Vol. 123, No. 5, 1997, pp. 405–413.

[3] Mull, M. A., Stuart, K., and Yehia, A., "Fracture Resistance Characterization of Chemically Modified Crumb Rubber Asphalt Pavement," *J. Mater. Sci.*, Vol. 37, 2002, pp. 557–566.

[4] Kim, K. W., Kweon, S. J., Doh, Y. S., and Park, T. S., "Fracture Toughness of Polymer-Modified Asphalt Concrete at Low Temperatures," *Can. J. Civil Eng.*, Vol. 30, 2003, pp. 406–413.

[5] Li, X. and Marasteanu, M. O., "Cohesive Modeling of Fracture in Asphalt Mixtures at Low Temperatures," *Int. J. Fract.*, Vol. 136, 2005, pp. 285–308.

[6] Song, S. H., Paulino, G. H., and Buttlar, W. G., "A Bilinear Cohesive Zone Model Tailored for Fracture of Asphalt Concrete Considering Viscoelastic Bulk Material," *Eng. Fract. Mech.*, Vol. 73, 2006, pp. 2829–2847.

[7] Kim, Y., Allen, D. H., and Little, D. N., "Computational Constitutive Model for Predicting Nonlinear Viscoelastic Damage and Fracture Failure of Asphalt Concrete Mixtures," *Int. J. Geomech.*, Vol. 7, No. 2, 2007, pp. 102–110.

[8] Kim, H. and Buttlar, W. G., "Discrete Fracture Modeling of Asphalt Concrete," *Int. J. Solids Struct.*, Vol. 46, 2009, pp. 2593–2604.

[9] Aragão, F. T. S., Kim, Y., Lee, J., and Allen, D. H., "Micromechanical Model for Heterogeneous Asphalt Concrete Mixtures Subjected to Fracture Failure," *J. Mater. Civil Eng.*, Vol. 23, No. 1, 2011, pp. 30–38.

[10] Song, S. H., Wagoner, M. P., and Paulino, G. H., "δ_{25} Crack Opening Displacement Parameter in Cohesive Zone Models: Experiments and Simulations in Asphalt Concrete," *Fatigue Fract. Eng. Mater. Struct.*, Vol. 31, 2008, pp. 850–856.

[11] Li, X. and Marasteanu, M. O., "The Fracture Process Zone in Asphalt Mixture at Low Temperature," *Eng. Fract. Mech.*, Vol. 77, 2010, pp. 1175–1190.

[12] Seo, Y., Kim, Y. R., and Witczak, M. W., "Application of the Digital Image Correlation Method to Mechanical Testing of Asphalt-Aggregate Mixtures," *Transport. Res. Rec.*, Vol. 1789, 2002, pp. 162–172.

[13] Kim, Y. R., Daniel, J. S., and Wen, H., "Fatigue Performance Evaluation of WestTrack Asphalt Mixtures Using Viscoelastic Continuum Damage Approach," *Final Report No. FHWA/NC/2002-004*, North Carolina State University, 2002.

[14] AASHTO TP62-07, "Determining Dynamic Modulus of Hot-Mix Asphalt Concrete Mixtures," *Standard Specifications for Transportation and Methods of Sampling and Testing*, 28th ed., America Association of State Transportation and Highway Engineering, 2008.

[15] Hoare, T. R. and Hesp, S., "Low-Temperature Fracture Testing of Asphalt Binders: Regular and Modified Systems," *Transport. Res. Rec.*, Vol. 1728, 2000, pp. 36–42.

[16] Marasteanu, M. O., Dai, S. T., Labuz, J. F., and Li, X., "Determining the Low-Temperature Fracture Toughness of Asphalt Mixtures," *Transport. Res. Rec.*, Vol. 1789, 2002, pp. 191–199.

[17] Lee, N. K., Morrison, G. R., and Hesp, S., "Low Temperature Fracture of Polyethylene-Modified Asphalt Binders and Asphalt Concrete Mixes," *J. Assoc. Asphalt Paving Technol.*, Vol. 64, 1995, pp. 534–574.

[18] Wagoner, M. P., Buttlar, W. G., and Paulino, G. H., "Disk-Shaped Compact Tension Test for Asphalt Concrete Fracture," *Soc. Exp. Mech.*, Vol. 45, No. 3, 2005, pp. 270–277.

[19] Wagoner, M. P., Buttlar, W. G., Paulino, G. H., and Blankenship, P., "Laboratory Testing Suite for Characterization of Asphalt Concrete Mixtures Obtained from Field Cores," *J. Assoc. Asphalt Paving Technol.*, Vol. 75, 2006, pp. 815-852.

[20] Molenaar, A. A. A., Scarpas, A., Liu, X., and Erkens, S. M. J. G., "Semicircular Bending Test: Simple but Useful?" *J. Assoc. Asphalt Paving Technol.*, Vol. 71, 2002, pp. 794–815.

[21] Li, X. and Marasteanu, M. O., "Evaluation of the Low Temperature Fracture Resistance of Asphalt Mixtures Using the Semi-Circular Bend Test," *J. Assoc. Asphalt Paving Technol.*, Vol. 73, 2004, pp. 401–426.

[22] Van Rooijen, R. C. and de Bondt, A. H., *Crack Propagation Performance Evaluation of Asphaltic Mixes Using a New Procedure Based on Cyclic Semi-Circular Bending Tests. Pavement Cracking: Mechanisms, Modeling, Detection, Testing, and Case Histories*, CRC Press, Boca Raton, 2008, pp. 437–446.

[23] Aragão, F. T. S., "Computational Microstructure Modeling of Asphalt Mixtures Subjected to Rate-Dependent Fracture," Ph.D. dissertation, University of Nebraska, Lincoln, NE, 2011.

[24] Wagoner, M. P., Buttlar, W. G., and Paulino, G. H., "Development of a Single-Edge Notched Beam Test for Asphalt Concrete Mixtures," *J. Test. Eval.*, Vol. 33, No. 6, 2005, pp. 452–460.

[25] Marasteanu, M. O., Zofka, A., Turos, M., Li, X., Velasques, R., Li, X., Buttlar, W., Paulino, G., Braham, A., Dave, E., Ojo, J., Bahia, H., Williams, C., Bausano, J., Gallistel, A., and McGraw, L., "Investigation of Low Temperature Cracking in Asphalt Pavements: National Pooled Fund Study 776," *Final Report No. MN/RC 2007-43*, Minnesota Department of Transportation, Saint Paul, MN, 2007.

[26] Duan, K., Hu, X., and Wittmann, F. H., "Scaling of Quasi-Brittle Fracture: Boundary and Size Effect," *Mech. Mater.*, Vol. 38, 2006, pp. 128–141.

[27] Kim, H., Wagoner, M. P., and Buttlar, W. G., "Simulation of Fracture Behavior in Asphalt Concrete Using a Heterogeneous Cohesive Zone Discrete Element Model," *J. Mater. Civil Eng.*, Vol. 20, No. 8, 2008, pp. 552–563.

[28] Geubelle, P. and Baylor, J., "Impact-Induced Delamination of Laminated Composites: A 2D Simulation," *Composites Part B: Eng.*, Vol. 29, No. 5, 1998, pp. 589–602.

[29] Espinosa, H. D. and Zavattieri, P. D., "A Grain Level Model for the Study of Failure Initiation and Evolution in Polycrystalline Brittle Materials, Part I: Theory and Numerical Implementation," *Mech. Mater.*, Vol. 35, 2003, pp. 333–364.

[30] Aragão, F. T. S. and Kim, Y., "Mode I Fracture Characterization of Bituminous Paving Mixtures at Intermediate Service Temperatures," *Exp. Mech.*, doi: 10.1007/s11340-012-9594-4.

[31] Rahul-Kumar, P., Jagota, A., Benninson, S. J., Saigal, S., and Muralidhar, S., "Polymer Interfacial Fracture Simulations Using Cohesive Elements," *Acta Mater.*, Vol. 47, No. 15, 1999, pp. 4161–4169.

[32] Nguyen, T. D., Govindjee, S., Klein, P. A., and Gao, H., "A Rate-Dependent Cohesive Continuum Model for the Study of Crack Dynamics," *Comput. Methods Appl. Mech. Eng.*, Vol. 193, 2004, pp. 3239–3265.

[33] Marzi, S., Hesebeck, O., Brede, M., and Kleiner, F., "A Rate-Dependent Cohesive Zone Model for Adhesively Bonded Joints Loaded in Mode I," *J. Adhes. Sci. Technol.*, Vol. 23, 2009, pp. 881–898.

[34] Shen, B. and Paulino, G. H., "Direct Extraction of Cohesive Fracture Properties from Digital Image Correlation: A Hybrid Inverse Technique," *Exp. Mech.*, Vol. 51, 2011, pp. 143–163.

[35] Gain, A. L., Carroll, J., Paulino, G. H., and Lambros, J., "A Hybrid Experimental/Numerical Technique to Extract Cohesive Fracture Properties for Mode-I Fracture of Quasi-Brittle Materials," *Int. J. Fract.*, Vol. 169, 2011, pp. 113–131.